Effect of pre-oxide on Zircaloy-4 high temperature steam oxidation

Severine Guilbert, Alice Viretto, Jean Desquines, Christian Duriez

Effect of pre-oxide on Zircaloy-4 high temperature steam oxidation

Guilbert-Banti S.[1*], Viretto A. [1], Desquines J. [1], Duriez C. [1]

[1] Institut de Radioprotection et de Sûreté Nucléaire, PSN-RES/SEREX/LE2M, Cadarache BP3, F-13115 Saint Paul lez Durance, France

*Corresponding author

E-mail address: severine.guilbert@irsn.fr

ABSTRACT:

An experimental study has been carried out on the high temperature oxidation behavior of pre-oxidized Zircaloy-4. Prior to steam oxidation, cladding tubes have been pre-oxidized in moistened oxygen environment at 425°C, up to pre-oxide layer thicknesses of 36 and 63 µm. All samples have then been subjected to isothermal high temperature steam oxidation, in the 900°C-1200°C temperature range, followed by water-quenching. Metallographic examinations and mean hydrogen content measurements have then been performed. For all tested temperatures, the weight gains measured for pre-oxidized samples are lower than those obtained for bare cladding, indicating that the pre-oxide has a protective effect against oxidation at high temperature. The results obtained on the O_2+steam pre-oxidized samples are in good agreement with published data on autoclave-pre-oxidized samples.

Comparison with literature data obtained on irradiated cladding shows that, at 1000°C and 1200°C, laboratory-grown unirradiated pre-oxidation layers have a stronger protective influence than a corrosion layer formed under irradiation. This difference in protectiveness may be explained by a more heterogeneous oxide microstructure and a higher intergranular porosity for in-reactor corrosion in comparison with laboratory pre-oxidation conditions.

KEYWORDS: LOCA, corrosion layer, steam oxidation, high temperature

1 INTRODUCTION

Under a loss-of-coolant-accident (LOCA), the fuel cladding is submitted to a rapid temperature increase (possibly up to 1200°C) in steam environment, inducing a high temperature oxidation until quenching occurs due to reflooding by the emergency core cooling system operation (ECCS). Acceptance criteria defined in 1973 by the US-AEC limit the cladding temperature to 2200°F (1204°C) and the oxidation amount to 17% ECR (Equivalent Cladding Reacted)[1] in order to prevent excessive embrittlement of the fuel cladding and to maintain a coolable geometry of the reactor core. These criteria were derived from mechanical testing of as-received cladding tubes after oxidation in steam atmosphere. However, the influence of the oxide layer formed on the outer cladding surface during the normal reactor operation (so called corrosion layer) has also to be taken into account. The thickness of this corrosion layer can reach at high burnup several tens of microns depending on the cladding alloy and the considered position along the fuel assembly.

Therefore, the influence of the pre-oxide layer on the high temperature steam oxidation of Zircaloy was addressed by several authors [1-7] and a review of the data available in the literature was recently published by Le Saux [8]. The main conclusions were that high temperature (HT) steam oxidation is generally delayed in the presence of a pre-oxide layer. This protective influence seems to increase with the increase of the pre-oxide scale thickness, and is observed to be less effective at 1200°C than at lower temperatures.

The basic principles of metal oxidation at elevated temperatures are described in [9]. The high temperature oxidation process is observed to be a two-step mechanism, showing first a reduction of the pre-oxide layer thickness, and later formation of high temperature oxide underneath the pre-oxide scale. This two-step mechanism can be explained as follows: after low temperature pre-oxidation, 1) the pre-oxide layer is stoichiometric for most of its thickness, and 2) the amount of oxygen dissolved in the metal is low, because the oxygen-enriched αZr(O) layer is very thin (typically less than 1 μm). When the cladding is heated at high temperature, the metal has the ability to dissolve a much higher amount of oxygen, which is a strong driving force for oxygen to migrate from the pre-oxide to the metal. A high oxygen flux crosses the metal/oxide (M/O) interface, the αZr(O) layer grows while the pre-oxide becomes sub-stoichiometric[2], starting from the M/O interface region. To put it another way, an oxygen vacancy gradient progressively establishes between the M/O interface and the oxide surface. As far as the gradient has not reached the surface, the oxygen flux incorporated from the atmosphere remains low (and the weight gain as well), the oxide is protective. Depending on the temperature and on the scale thickness, this situation is maintained during a sufficiently long period to convert oxide into metal at the M/O interface, and the pre-oxide scale thickness decreases. Once the sub-stoichiometry has reached the oxide scale surface (as revealed by the color change from the originally bright zirconia into black zirconia) incorporation and transport of oxygen from the steam environment is made possible and the vacancies concentration gradient reaches a steady state. As an illustration, for this steady state distribution of oxygen across the zirconia layer, Cathcart and Pawel considered a linear distribution with a close to stoichiometric concentration in the zirconia at the steam-oxide interface [10]. Because increase of the αZr(O) layer thickness progressively lowers the driving force for oxygen diffusion into the metal, the oxygen fluxes balance (flux at the M/O interface versus the flux at the surface) reverses and new oxide can form at the M/O interface. Modelling this complex multilayered configuration by solving the diffusion equations does predict this sequence of successive pre-oxide dissolution and later high temperature oxide formation [11].

Note that for thick corrosion layers having radially oriented cracks, HT oxide formation is observed to initiate first beneath these cracks, probably meaning that the vacancies gradient establishes faster there [2].

The above conclusions were derived from oxidation tests performed with various pre-oxidation conditions, and for pre-oxidation layers generally thinner than about 50 μm. We had observed in our laboratory, testing samples pre-oxidized in dry oxygen, a partial loss of protectiveness above a 40 μm pre-oxide thickness [12]. In the present study, the pre-oxidation conditions have been improved by adding a controlled steam amount in the pre-oxidation furnace, to reproduce the Zircaloy-4 hydrogen charging effect observed during in-reactor

---

[1] This parameter is defined as the ratio between the weight gain versus its maximum possible value corresponding to full oxidation of the sample. It may also be expressed as the ratio between the mass of reacted metal layer to the metal mass before oxidation.

[2] The Zr-O phase diagram allows significant deviation from stoichiometry for zirconia at high temperature, see Ma, X., et al., Journal of Nuclear Materials, 2008. **377**(2): p. 359-369.

corrosion. For a better understanding of the pre-oxide layer thickness influence, 2 different thicknesses have been considered, up to 63 µm to account for high burnup fuels.
The objectives of this paper is first to compare the HT oxidation behavior of samples pre-oxidized in O_2+steam and in autoclave. As it is rarely presented in the literature, the second objective is to compare the behavior at high temperature of out-of-pile and in-pile corroded material. The paper is organized as follows. The microstructure and morphology of the pre-oxidation layers formed in O_2+steam are first presented. Then, they are compared to those formed in autoclave conditions. Next, high temperature oxidation results, obtained at 900, 1000, 1100 and 1200°C on the O_2+steam pre-oxidized samples are discussed in terms of weight gain, oxide scale thickness and hydrogen pick-up as well. At last, comparison is made with data obtained in other laboratories with autoclaved specimens, and with irradiated cladding when available.

2 MATERIALS AND METHODS

2.1 Materials

The specimens used in this study were cut from low tin Stress-Relieved Annealed (SRA) Zircaloy-4 PWR 17x17 industrial fuel cladding tubes, provided by AREVA-NP. Composition of the alloy is given in Table 1. Outer diameter and wall thickness of the tubes are 9.5 mm and 570 µm respectively. Open samples were used, leading thus to two-side oxidations.

Sn (wt%)	Fe (wt%)	Cr (wt%)	O (wt%)	H (wtppm)
1.3	0.21	0.10	0.13	10

Table 1: Chemical composition of the Zry-4 batch used for pre-oxidation in moistened oxygen

For pre-oxidation, 100 mm long cladding samples were heated at 425°C in a tubular resistive furnace in a flowing mixture of oxygen and steam (3 $NL.h^{-1}$ O_2 + 15% vol. steam), for respectively 212 and 385 days. The steam partial pressure was adjusted to reach respectively about 300 and 400 wtppm hydrogen incorporation at the end of the pre-oxidation periods. The pre-oxidation temperature is lower than the temperature of the final fabrication heat treatment of the alloy, and no or only partial recrystallization is expected during pre-oxidation. End's part of the pre-oxidized samples are used for metallography and hydrogen measurements. The central part is cut in 20 mm long samples for the HT steam oxidation.

2.2 Steam oxidation at high temperature

Oxidation in this study was performed at 900°C, 1000°C, 1100°C and 1200°C at atmospheric pressure in a vertical resistive furnace in a steam + argon flow (with a heating rate of ~ 50°C.s^{-1}) on 20 mm long samples, oxidized on both the outer and the inner surface (two-side oxidation). As the 20 mm long samples are cut from the 100 mm pre-oxidized specimens, sample ends are bare before HT oxidation. This may lead to an overestimation of the weight gain of pre-oxidized samples. However, end's area represents only 2% of the total exposed area and the contribution of this bare area to the weight gain is negligible. Holding time ranged between 5 min and 100 min depending on the temperature. Samples were then water-quenched by dropping into a water bath. The argon and steam flow rates were respectively 120 $Nl.h^{-1}$ and 100 $g.h^{-1}$ between 900 and 1100°C, corresponding to a 50/50 Ar/steam vol. fraction (pH_2O = 510 hPa[3]). At 1200°C, the argon and steam flow were increased to 600 $Nl.h^{-1}$ and 500 $g.h^{-1}$ to avoid any occurrence of steam starvation. The steam flow rate normalized to the cross-sectional area of the furnace alumina tube was thus respectively 3.9 $mg.cm^{-2}.s^{-1}$ at 900°C-1100°C and 19.6 $mg.cm^{-2}.s^{-1}$ at 1200°C. Prior the tests on pre-oxidized cladding, a test campaign was performed on as-received samples and hydrogen content was measured systematically after HT steam oxidation in order to confirm that these experimental conditions prevent steam starvation. Indeed,

[3] The partial pressure is calculated on the basis of a 1000 hPa total pressure.

Brachet [13] and Uetsuka [14, 15] showed that hydrogen uptake was observed for stagnant or flowing hydrogen enriched steam conditions.

2.3 Sample characterizations

Weight and length of the samples were measured with an accuracy of 0.1 mg and 0.01 mm respectively, before and after pre-oxidation and HT oxidation. The weight gain was calculated from these measurements. After each step of the preparation protocol, samples were cut and embedded in epoxy resin, ground and polished. Polishing was performed with SiC papers, diamond paste and finally colloidal silica suspensions. Metallographic cross sections were examined by optical microscopy (Keyence digital microscope). Each oxide layer thickness and standard deviation was determined from a set of 12 measurements performed on both outer and inner surfaces on 2 metallographic radial cuts (3 regularly-spaced measurements at 4 different angular locations). Scanning Electron Microscopy (SEM) images were obtained with a field-emission SEM (Zeiss SIGMA 500 VP) equipped with a backscattered electron detector.
Hydrogen contents were measured by the hot extraction technique (analyzer system JUWE ON/H-mat 286). For each sample, measurements were repeated at least three times on small pieces of few tens of mg on two different rings after sand-blasting the oxide layer. As mentioned later (see §3.1), the hydrides are homogenously distributed, and thus the sand-blasting does not affect the measured hydrogen content. However, sand-blasting might remove partly the αZr(O) layer. Because this αZr(O) layer is known to be hydrogen-depleted, its removal may lead to a slight over-estimation of the mean hydrogen content in the metal after HT oxidation. The hydrogen pickup during HT oxidation was calculated as the difference of hydrogen content measured after steam oxidation and the one measured after pre-oxidation.
Microhardness measurements were performed using a BUEHLER apparatus equipped with a Vickers diamond tip. A 100g load was used. On each metallographic cut, four profiles were measured across sample radius in the metal with 100 µm spacing between indentation marks.
Raman scattering measurements were performed using a RM1000 Renishaw spectrometer. It was equipped with an air-cooled CCD detector and a microscope. The excitation wavelength was the 514 nm line of an Ar+ ion laser. The power at the specimen was a few mW. The sample were examined with a point spacing of 1 µm.

3 EXPERIMENTAL RESULTS

3.1 Pre-oxidation

Specimens were pre-oxidized up to an oxide layer mean thickness of 35.7 ± 4.4 µm and 63.2 ± 7.5 µm. Examples of micrographs and metallographs are presented on FIG 1 and FIG 2. Vickers micro-hardness measurements indicated flat profiles in the metal part of the pre-oxidized samples (measurements not shown). The mean values appears slightly lower than the one measured for the as-received alloy (222 ± 29 Hv0.1 and 216 ± 28 Hv0.1 respectively for the 36 µm and 63 µm thick pre-oxide layers to compare to 232 ± 30 Hv0.1 for as-received alloy). These lower values are the result of the long term treatment at 425°C, however, it remains higher than in fully recrystallized Zircaloy (191 ± 32 Hv0.1), indicating that recrystallization at 425°C is only partial.

After the pre-oxidation, the samples color is light brown (FIG 1). The brown color may come from the ferrite oxide after oxidation of the SPPs (Second Phase Particles). A network of axial-radial cracks is observed at the outer surface for both pre-oxide thickness (FIG 1). The metallographic cross sections (FIG 3 (a)) show the presence of a zirconia layer with the typical stratified microstructure of zirconium alloys [16-18]. The strata are defined by circumferential cracks parallel to the metal/oxide interface. Strata thickness is approximately 2-3µm. Radially oriented veins, where the oxide is dense and free of cracks, are also observed. A network of regularly spaced radial cracks is observed at the outer side. They correspond to the axially oriented cracks observed at the sample surface. Such cracks are not observed on the inner side. The grains are columnar and elongated in the growth direction. Their length and width were
estimated to be few hundred µm and few tens of µm respectively.
At high magnification, FEG-SEM images show that besides the circumferential cracks,

the oxide contains numerous nano and micro-cracks or pores (FIG 3 (b-c)). In the metal, the hydrides are homogeneously distributed and rather circumferentially oriented (FIG 2). The mean hydrogen content is 272±42 wtppm and 402±37 wtppm, respectively for the 36 µm and 63 µm thick pre-oxide layers.

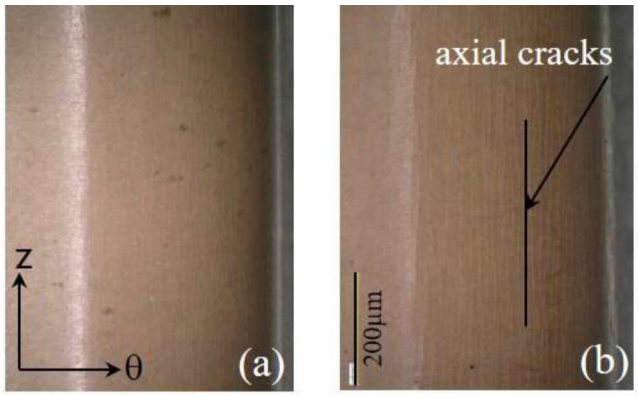

FIG 1: Binocular images of the outer surface of O_2+steam pre-oxidized samples after pre-oxidation at 425°C, (a) pre-oxide mean layer thickness 36 µm, (b) pre-oxide mean layer thickness 63 µm

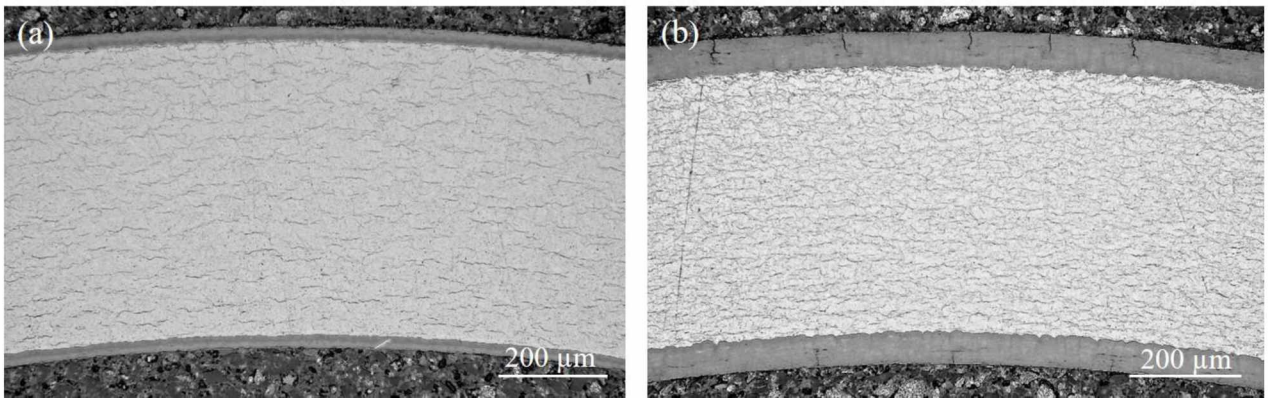

FIG 2: Metallographic cross section after hydride etching (optical microscopy) (a) pre-oxide mean layer thickness 36 µm, mean hydrogen content 272±42 wtppm (b) pre-oxide mean layer thickness 63 µm, mean hydrogen content 402±37 wtppm

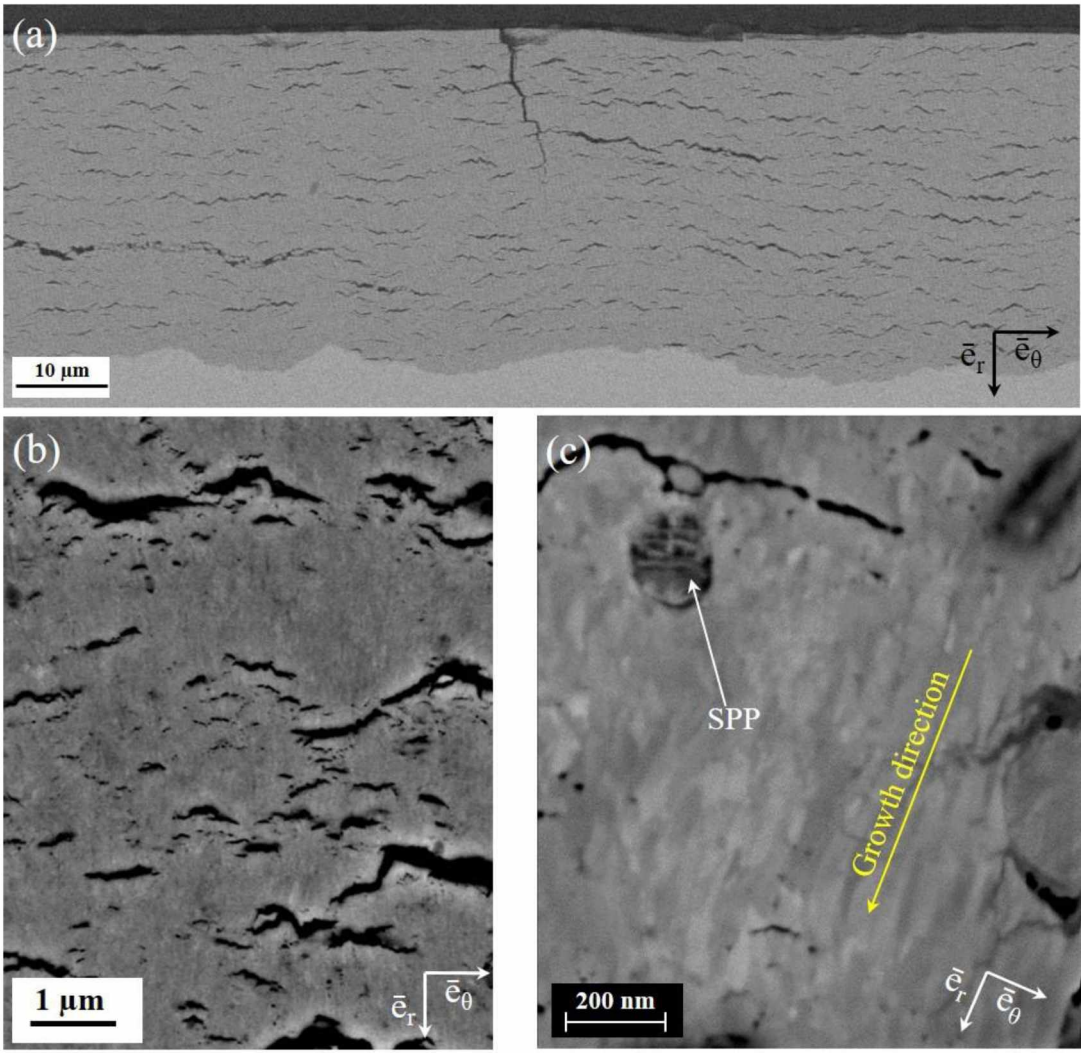

FIG 3: FEG-SEM/BSE images of O_2+H_2O pre-oxidized Zry-4 cladding cross section (pre-oxide thickness 36 µm): (a) low magnification, outer side; (b) and (c) high magnification

Raman imaging was used after pre-oxidation to examine the zirconia layers on metallographic cross-section. This technique can give information on the oxide stoichiometry. Indeed, the scattered intensity is sensitive to the crystallinity of the oxide and intensity variations can be interpreted in term of stoichiometry changes [19]. So, by following a given peak of the monoclinic zirconia, it is possible to obtain a qualitative oxide stoichiometry map. The intensity of the 475 cm^{-1} Raman peak, one of the main bands of monoclinic zirconia, was mapped after O_2+steam pre-oxidation and plotted in a log scale on FIG 4 a. This figure shows that the Raman signal is intense on almost all the thickness of the oxide layer, which is indicative of a high crystallinity and likely of a stoichiometric oxide. Only the last strata close to the metal/oxide interface exhibits a strong decrease of the 475 cm^{-1} line, probably linked to a sub-stoichiometric layer. The thickness of this last strata, about 2-3 µm, is significantly larger than the size of the Raman laser probe, estimated to be 0.5 µm. Therefore, the intensity decrease observed cannot be attributed to probe overlapping with the nearby metallic substrate, and is rather a signature of sub-stoichiometry of this last strata.

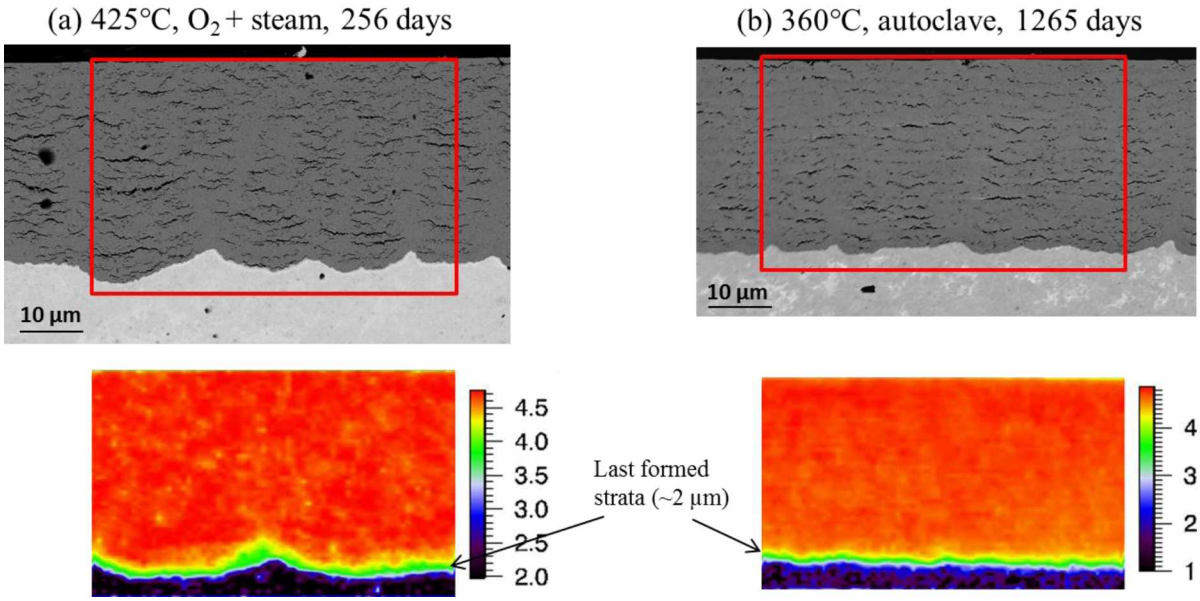

FIG 4: SEM image and 475 cm^{-1} line integrated intensity map (log scale) in the oxide layer (a) after O_2+steam at 425°C pre-oxidation and (b) after autoclave pre-oxidation

3.2 Comparison with autoclave pre-oxidized cladding

Pre-oxidation is, most of the time, performed in static water at 340-360°C with a typical PWR primary water chemistry [8, 17, 20-22]. This kind of experimental conditions is supposed to produce a pre-oxidized cladding representative of the irradiated materials. This paragraph synthetizes the observations reported in the literature on autoclave pre-oxidized cladding, in terms of microstructure and hydride distribution. The characteristics of O_2+steam pre-oxidized and autoclave pre-oxidized samples are then compared.

Examinations of radial cross-sections of Zry-4 after corrosion under static pressurized water at 360°C show similar features as the O_2+steam pre-oxidized samples: stratified microstructure with 2µm-thick strata, presence of radially-oriented veins, and radial cracks in the outer part of the layer for thick pre-oxide layers (>30µm) (FIG 5) [8]. High magnification FEG-SEM image also reveals that the autoclave-formed oxide contains numerous nano and micro-cracks [12] (FIG 6). The oxide is formed mostly of columnar grains oriented perpendicular to the metal/oxide interface and of equiaxed grains. The equiaxed grains have a more random orientation according to EBSD measurements [20]; the length of the columnar grains is ~100 to 300 nm and the diameter of the equiaxed and the columnar grains is less than 50 nm [17, 20, 21]. As for O_2+steam pre-oxidized samples, Raman map of the 475 cm^{-1} line intensity shows an intense Raman signal on almost all the oxide thickness, except for the last strata (FIG 4 (b)).

Corrosion in autoclave leads also, as pre-oxidation in O_2+steam, to circumferential homogeneous hydride distribution in the metal, due to the absence of temperature gradient across the cladding wall.

Thus, Zry-4 cladding pre-oxidized under O_2+steam at 425°C has a number of similarities with cladding corroded in autoclave: stratified microstructure defined by circumferential cracks parallel to the metal/oxide interface, nano and micro-cracks beneath the circumferential cracks, radially oriented veins, radial cracks for high pre-oxide thickness, homogeneous distribution of circumferential hydrides, columnar grains of similar size, stoichiometric oxide on almost all the oxide thickness. This may suggest a comparable oxide growth mechanism for the two pre-oxidation conditions.

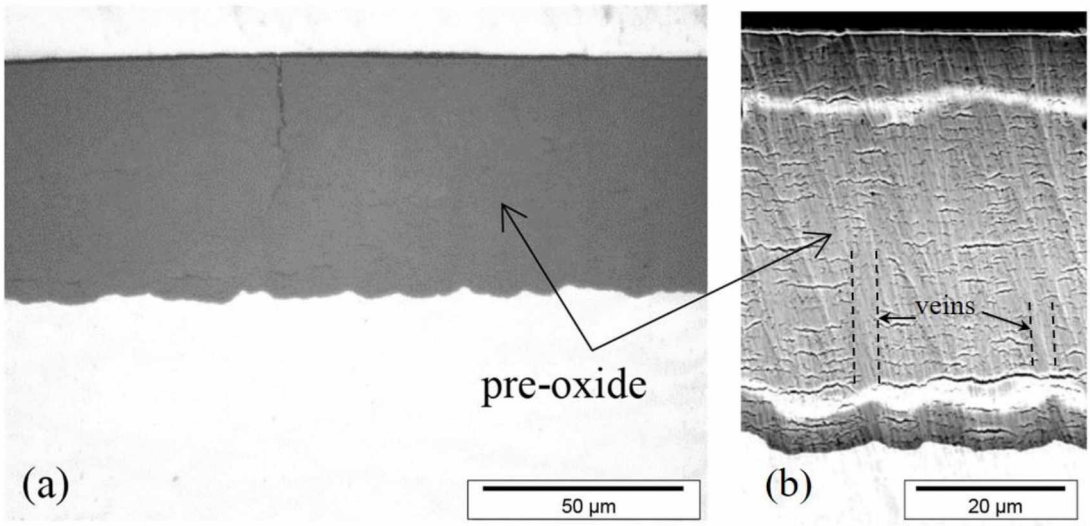

FIG 5: (a) Metallographic cross-section image and (b) SEM image of radial cross-section of Zry-4 cladding after corrosion under static water at 360°C, outer side, pre-oxide thickness 59 µm [8]

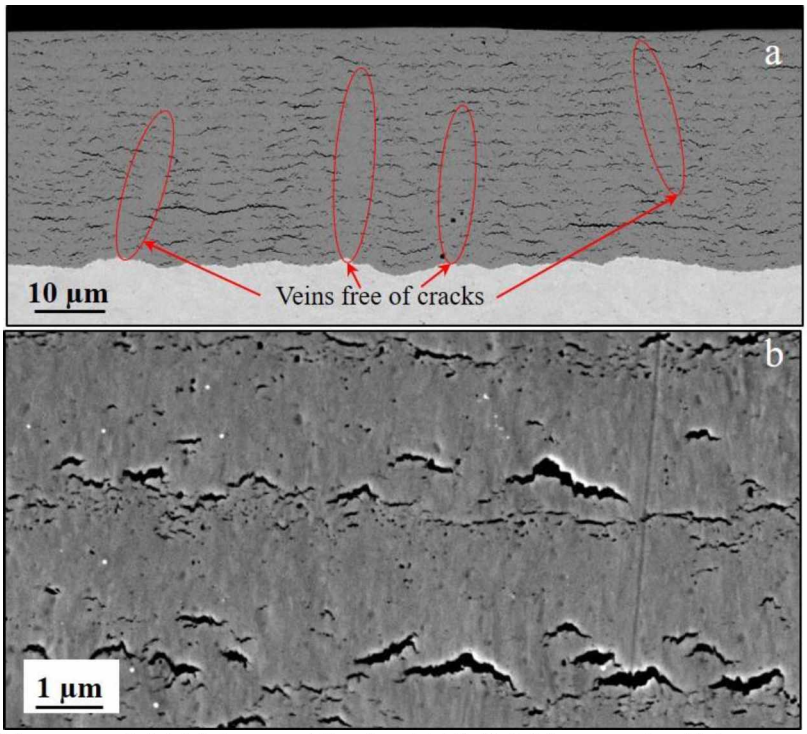

FIG 6: (a) SEM image and (b) high magnification FEG-SEM image of radial cross-section of Zry-4 cladding after corrosion under static water at 360°C for 1440 days. SEM images obtained on an autoclaved sample provided by EDF [12]

3.3 High Temperature Steam Oxidation of Bare Cladding Samples

To qualify the furnace and the oxidation protocol in terms of oxidation kinetics, results obtained at 900°C, 1000°C, 1100°C and 1200°C on Zry-4 as-received samples were compared to published data (FIG 7). In this figure, the Cathcart-Pawel correlation (CP) is reported for 1000°C, 1100°C and 1200°C. At 900°C, the parabolic CP correlation is known to be no more valid [22] and a cubic correlation was used instead. The results are in good agreement with the published data, and the parabolic or cubic correlations. Furthermore, negligible hydrogen pick-up was measured on these samples (<30wppm); significant hydrogen pick-up would have suggest steam starvation, as mentioned previously. At last, outer and inner oxide thickness were

measured after HT steam oxidation. A good agreement is observed between the two (see FIG 8 for instance at 1000°C), indicating that the atmosphere inside and outside the sample is the same. Thus, the relevance of the experimental protocol adopted for this study is demonstrated.
One can note large discrepancies in the experimental data at 1000°C for the longer durations. The incubation period for breakaway oxidation is the shortest at this temperature [23]. The increase in the oxidation rate and the hydrogen pickup associated to breakaway oxidation can enhance deterioration of the mechanical properties of the cladding and the discrepancies in weight gain might be explained by a partial spalling of the oxide layer.

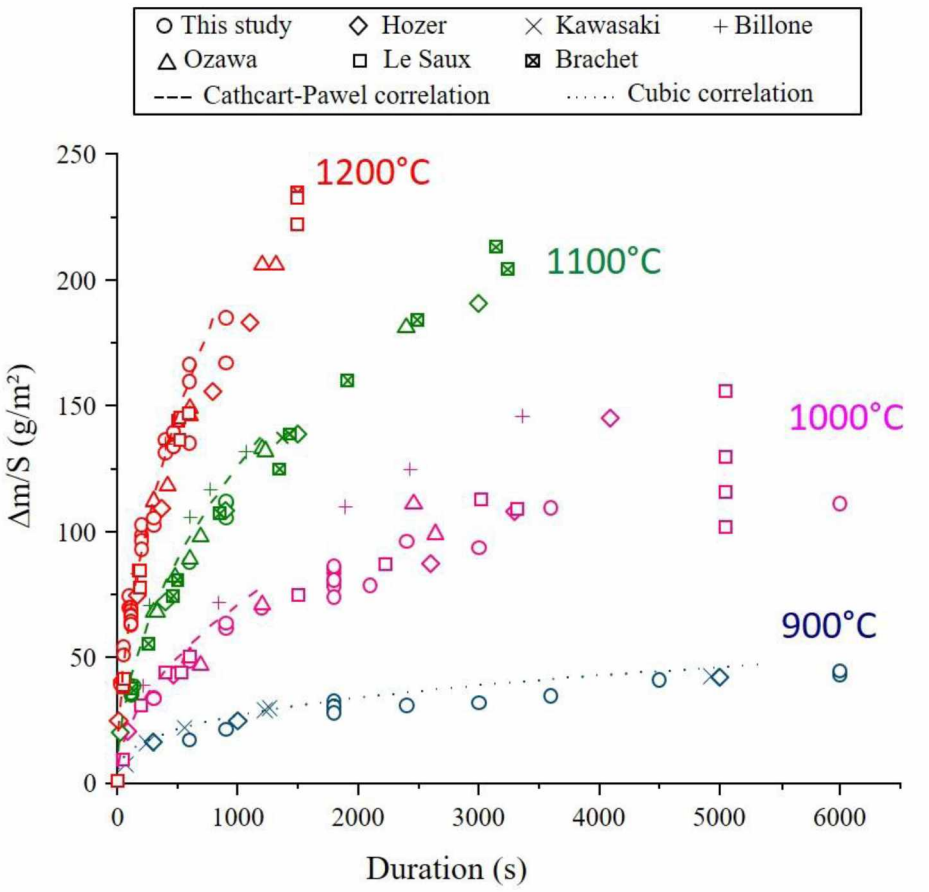

FIG 7: Weight gain as a function of time for steam oxidation of as-received samples. Comparison with data by Hozer [24], Kawasaki [22], Billone [25], Ozawa [26], Le Saux [8] and Brachet [27]

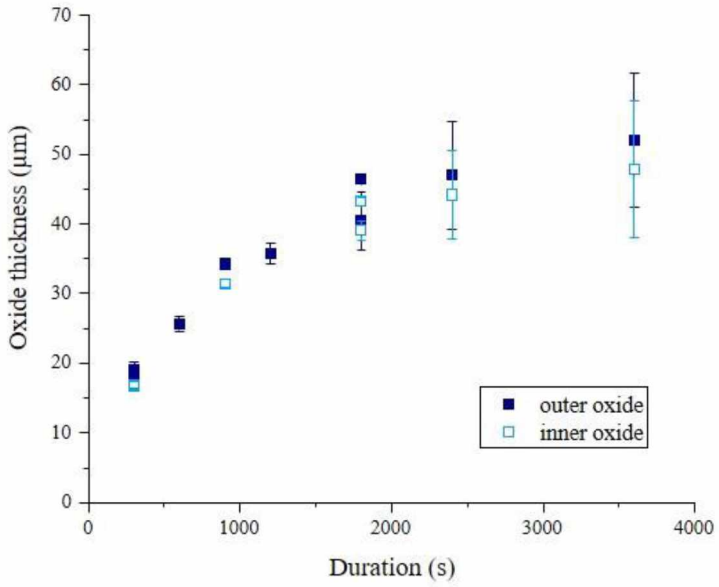

FIG 8: Outer and inner oxide thicknesses after steam oxidation of as-received cladding at 1000°C

For initially bare samples, after HT steam oxidation, metallographic cross sections show the presence of a dense and uniform oxide on both the inner and the outer sides, for all temperature and duration investigated (see for example the metallographs after oxidation at 1000°C on FIG 9). The morphology of the oxide is typical of a pre-breakaway oxidation regime. At 1000°C and after 30 min, undulations of the oxidation front are likely indicative of a close breakaway transition. Indeed, 1000°C appears to be a temperature with maximized sensitivity to breakaway oxidation [28]. In any case, the hydrogen pickup during the steam oxidation remains low (~5-10 wtppm), which is also consistent with a pre-breakaway regime.

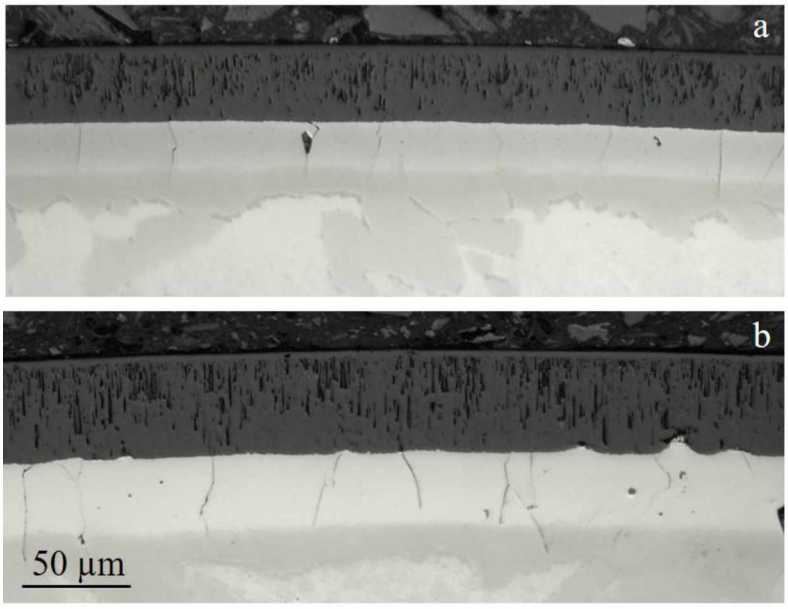

FIG 9: Metallographic cross section image of bare Zry-4 after steam oxidation at 1000°C for (a) 15 min and (b) 30 min

3.4 High temperature steam oxidation of pre-oxidized cladding samples

Weight gain and oxide morphology - For the 36 μm pre-oxide layer, sample color, which was light brown after the pre-oxidation, has turned to a mix of black and beige areas (FIG 10). Proportions of black and beige areas depend on temperature and oxidation duration: the proportion of black areas decreases with duration and increases with temperature, except at 1200°C, where on the contrary it increases with time. For the thicker pre-oxide layers (63 μm), the beige color covers the entire sample surface, at 900°C-1000°C, whereas at 1100°C-1200°C, there is still a small proportion of black areas. The black color at the surface of the samples indicates that the pre-oxide layer has become sub-stoichiometric up to its surface, while beige regions correspond to area where the oxide is stoichiometric, at least at the surface.
The weight gained by O_2+steam pre-oxidized Zircaloy-4 cladding during the HT oxidation at 900-1200°C is plotted in FIG 11 as a function of the square root of oxidation time. The weight gains of as-received Zry-4 reported by Le Saux [5, 8], by Narukawa [29], by Ozawa [26] and Kawasaki [22] are shown as reference, as well as the Cathcart-Pawel correlation [10]. The weight gain of autoclave pre-oxidized cladding is also reported in FIG 11 [5, 22, 26]. As shown in this figure, the results obtained on O_2+steam pre-oxidized cladding are in good agreement with results obtained on autoclave-pre-oxidized samples. The general trend for pre-oxidized samples, either in O_2+steam flux or in autoclave, is a much lower weight gain compared to as-received specimens, indication of the protective influence of these pre-oxide layers. However, the protective effect is observed to decrease as the oxidation temperature increases, and at 1200°C, the weight gains of pre-oxidized samples are nearly the same as the ones obtained on as-received specimens. Furthermore, for the same oxidations conditions (900°C, 100 min), FIG 12 shows that the protective effect increases with the pre-oxide thickness up to ~30μm and then seems to remain constant.
Examples of metallographic images obtained on cross-sections after steam oxidation for all tested conditions are displayed in FIG 9 and FIG 13.

They always show several layers after high temperature oxidation:

- a ZrO_2 oxide layer, consisting of the remaining pre-oxide and the oxide formed at HT,
- a bright metallic layer corresponding to the oxygen-stabilized αZr(O) layer,
- a prior-β layer or a two-phase α+prior-β layer depending on the temperature and on the oxygen and hydrogen contents.

The first two layers are found on both the inner and outer cladding surfaces for two-side oxidation. Examination of the optical microscopy images shows that the presence of HT oxide depends on the temperature and duration and also on the pre-oxide thickness: the higher the temperature, the sooner the HT oxide appears. For a given temperature, the HT oxide appears later for the thicker pre-oxide layer. It seems that HT oxide forms first as oxide nodules and later becomes a continuous layer if the oxidation duration is long enough. This process was already observed by Nagase and in a previous study [12, 30].
It is also interesting to note in FIG 14-b the presence of circumferential cracks at the O/M interface in the metal part. Similar cracks were already observed in a previous study [12] and were attributed to a conversion of a thin layer of pre-oxide into metal, leading to a setback of the metal/oxide interface. As a consequence, the circumferential cracks, which were initially in the pre-oxide layer are found in the metallic part. These circumferential cracks in the metal part are not observed at 1200°C. SEM images reveal that the metal grains in the region of oxide reduction are much smaller than away from the metal/oxide interface (FIG 14), likely because they have formed from the small-grained zirconia. Reduction zones may co-exist with regions where HT oxide has formed. It seems that oxide reduction happens preferentially in advances of the reaction front, leading to a flattening of the metal/oxide interface undulations.
The thickness of the HT oxide layer is calculated as the difference between the mean oxide thickness after steam oxidation and the mean pre-oxide thickness, both measured on optical cross section images, and plotted in FIG 15 as a function of the oxidation time for the tests performed at 900 and 1200°C. As depicted in this figure, the oxide thickness at the inner surface is always thinner than that of the outer surface, although it follows the same trend. It is likely due to compressive stresses which develop in the internal oxide sub-layer resulting in a slightly higher protective influence of the inner pre-oxide. Reduction of the pre-oxide layer is observed at 900°C-1100°C (FIG 13), whereas at 1200°C, this figure (FIG 13) shows high temperature oxidation. Due to the shorter protective period at 1200°C compared to lower temperature conditions, it was not possible to observe the reduction phase on metallographs at this temperature.

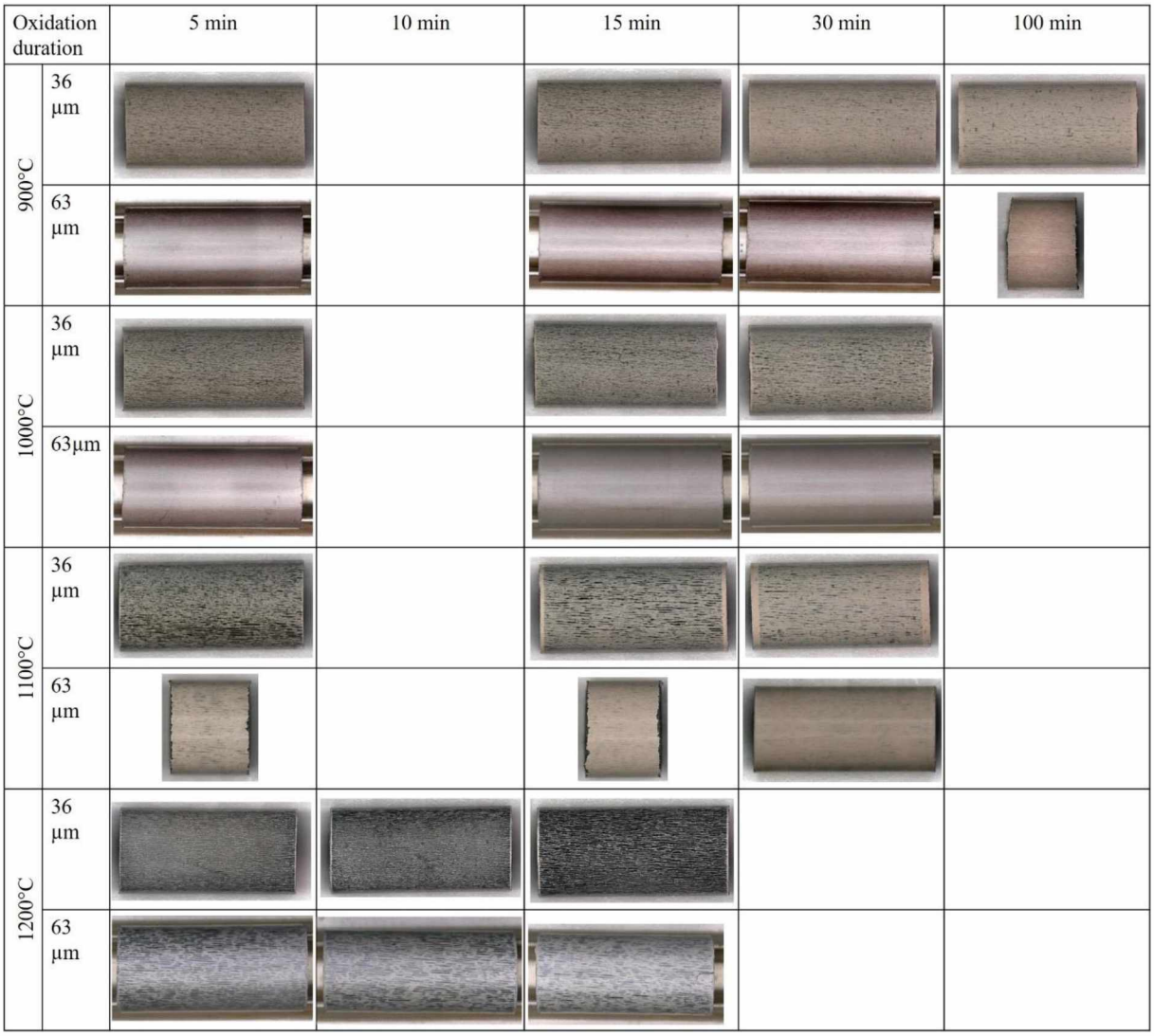

FIG 10: Binocular images of the outer surface of O_2+steam pre-oxidized samples after steam oxidation at high temperature.

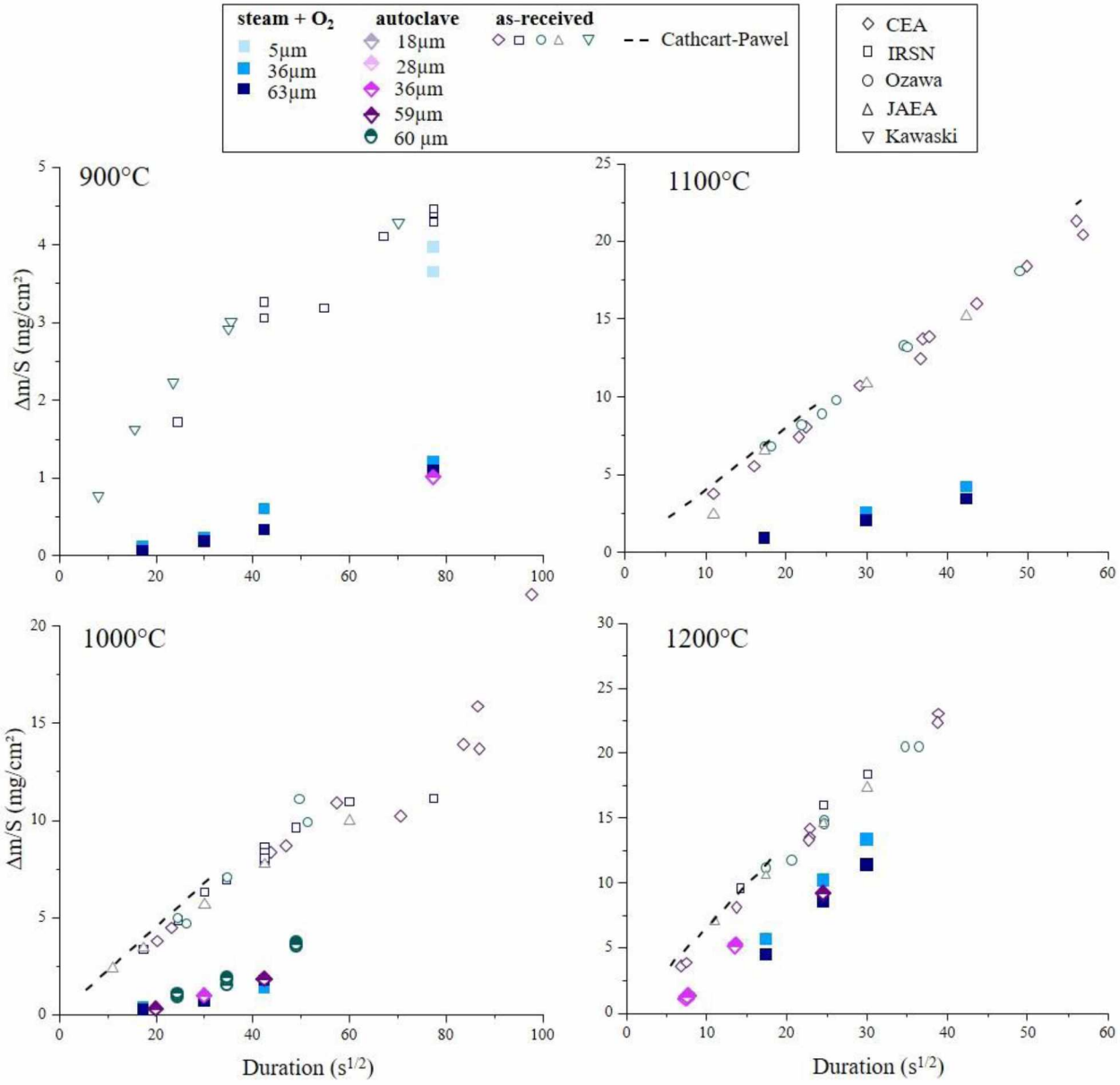

FIG 11: Weight gains of Zircaloy-4 after steam oxidation as a function of the square root of the oxidation time. Results from this study are compared to results obtained on as-received cladding by Le Saux [5, 8], Narukawa [29], Ozawa [26], Kawasaki [22] and on autoclave samples by Le Saux [5, 8].

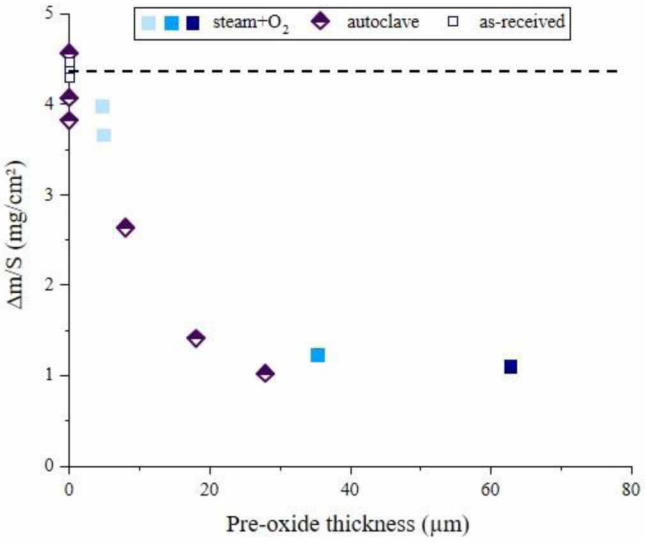

FIG 12: Weight gain of Zircaloy-4 after steam oxidation at 900°C for 100 min as a function of the pre-oxide thickness (similarly to Fig.8 - square symbols: IRSN tests - diamond symbols: CEA tests [5, 8]).

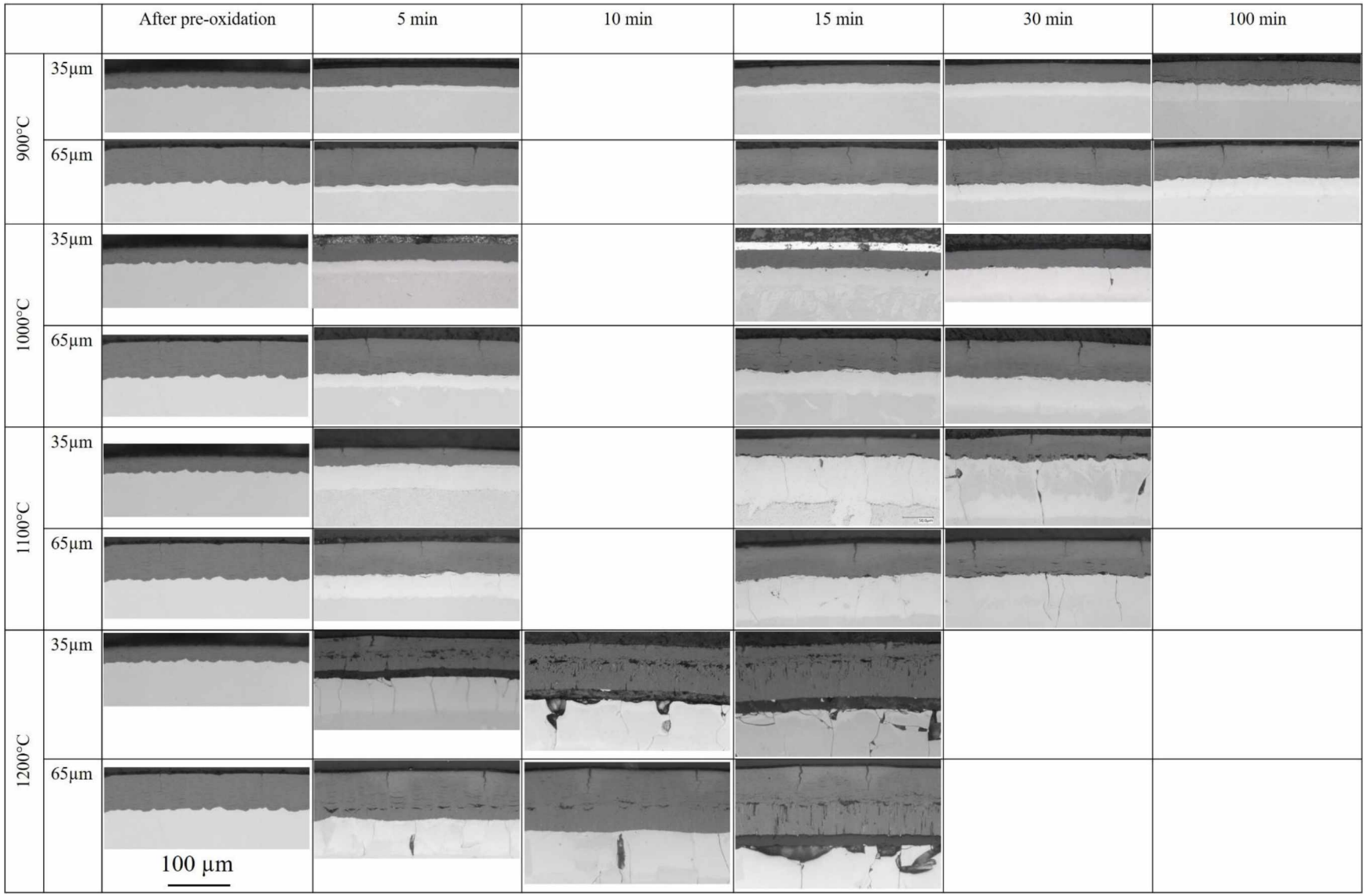

FIG 13: Optical images of cross-section of Zry-4 samples after steam oxidation at high temperature (same scale for all micrographs).

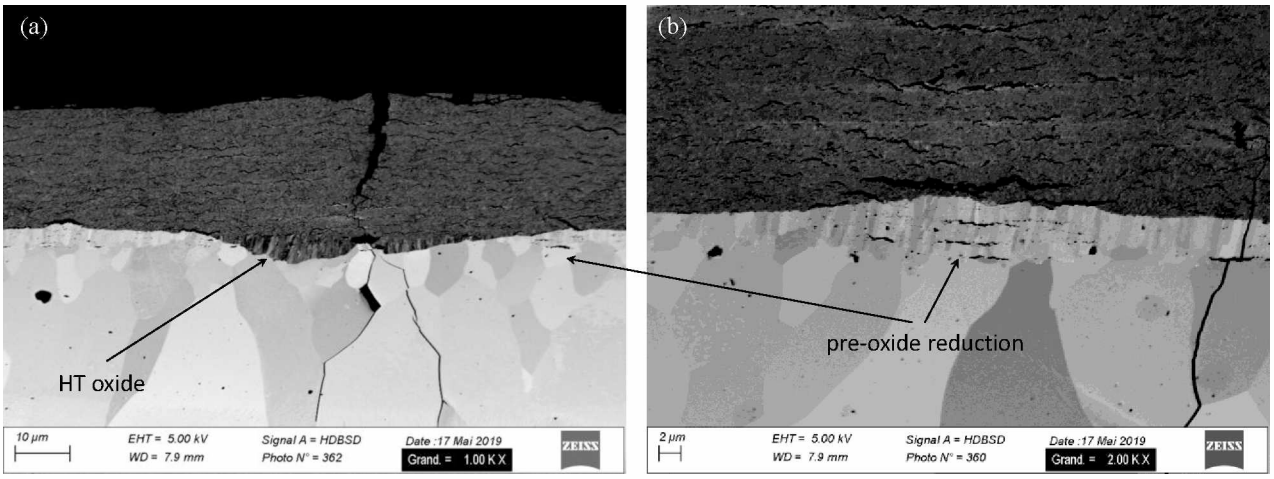

FIG 14: BSE/SEM images of transverse cross-section of Zry-4 sample after steam oxidation at 1000°C

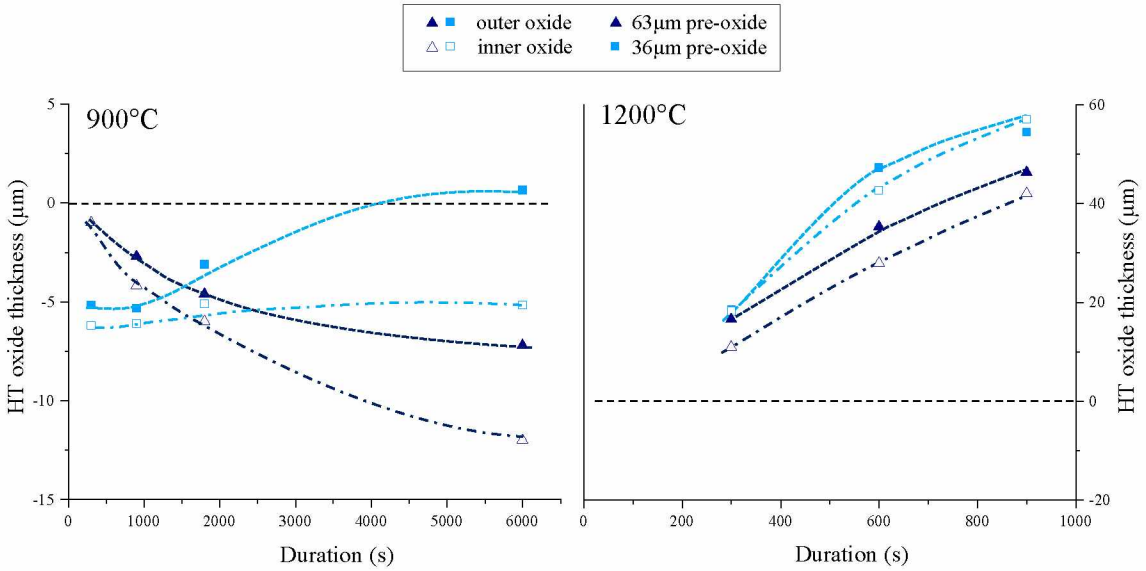

FIG 15: Total outer and inner HT oxide thickness as a function of the oxidation duration at 900°C and 1200°C.

Hydrogen pickup during the high temperature oxidation has also been investigated, by systematically measuring the samples hydrogen contents before and after the HT oxidation phase. This amount, presented in FIG 16 (a), was calculated as the difference between the hydrogen content after the HT oxidation and after the pre-oxidation. As shown in this figure, the hydrogen content remains low (< 200 wtppm) with an increasing trend with time, even at 1200°C, temperature at which high temperature oxide was observed. The hydrogen pickup fraction (HPUF), $f_{H\alpha}$ which is defined as the ratio of the hydrogen absorbed by the material over the total hydrogen generated during the oxidation was also calculated as follows [8]:

$$f_{H\alpha} = \frac{M_O}{2M_H} \frac{10^{-6} C_{H\alpha} m_t}{(1 - 10^{-6} C_{H\alpha}) m_t - m_{t_0}}$$

With:

$C_{H\alpha}$: the hydrogen content of the sample

M_O: the molar mass of oxygen

M_H: the molar mass of hydrogen

m_t: the total mass of oxidized sample

m_0: the sample mass before HT oxidation

As shown in FIG 16 (b), the hydrogen pickup fraction obtained on O_2+steam pre-oxidized samples is in good agreement with the HPUF calculated for autoclave samples, and remains rather low except at 900°C.

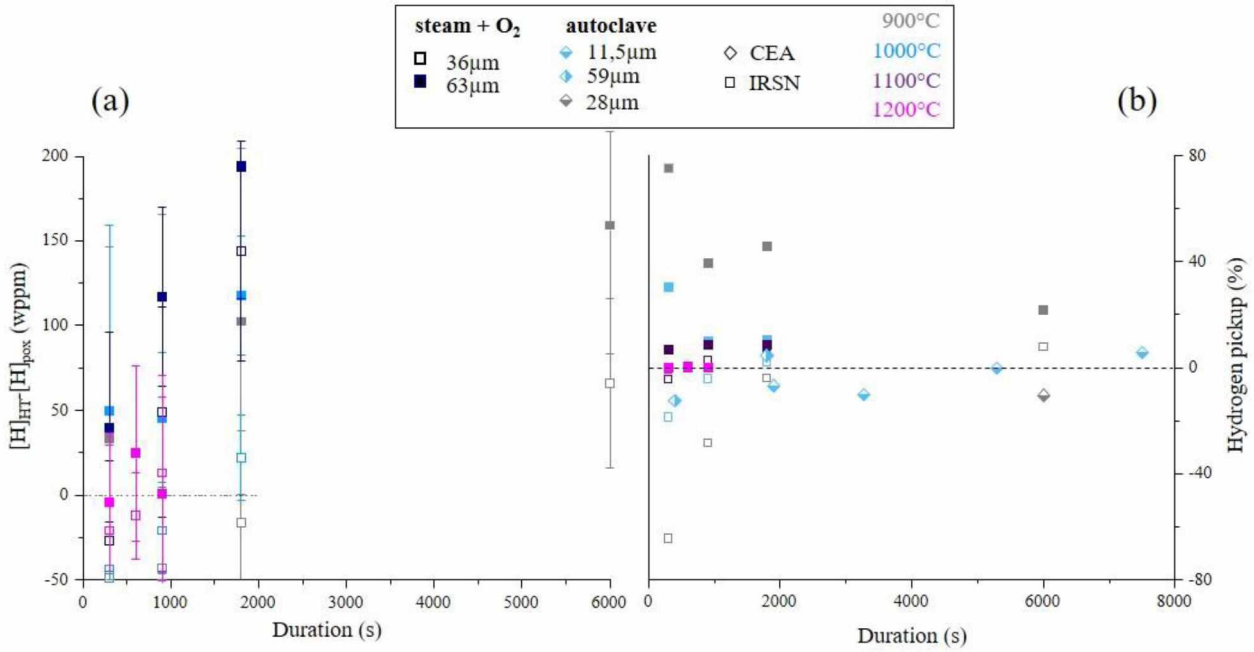

FIG 16: (a) Amounts of hydrogen absorbed by pre-oxidized Zry-4 cladding during steam oxidation, (b) hydrogen pickup fraction – comparison with autoclave data [8]

4 DISCUSSION

It is also interesting to compare these results with results obtained on irradiated Zry-4 cladding. However, data on the HT steam oxidation behavior of irradiated Zry-4 are rather scarce. Some tests were performed at ANL [25], but the oxidation temperature was restricted to 1200°C. In the recent years, JAEA has explored more systematically the influence of in-reactor corrosion on high temperature oxidation testing several irradiated cladding alloys [29, 31]. These results, even if not obtained with the Zircaloy-4 alloy, can also be considered in order to enrich the discussion.

The thicknesses of the HT oxide layers formed during the oxidation at 1000°C and 1200°C on irradiated cladding are presented and compared to results on lab-pre-oxidized specimens respectively on FIG 17 and FIG 18. As shown in these figures, the HT oxide thicknesses measured on irradiated cladding are lower than the ones obtained on as-received cladding, reflecting the protectiveness of the corrosion layer formed during normal operations. However, this protective effect is reduced at 1200°C. At this temperature, the influence of the alloy composition on the HT behavior of as-received cladding appears to be negligible, as the HT oxide thicknesses are of the same order of magnitude. The same trend is also observed on irradiated cladding and was already mentioned by Chuto [2, 29, 32]. Furthermore, the HT oxide thicknesses measured on irradiated cladding are very close to the ones obtained on as-received samples, which might be indicative of a loss of protectiveness of the corrosion layer at 1200°C.

By comparison, a laboratory-grown pre-oxidation layer, either in O_2+steam or in autoclave, has a more protective effect at 1000°C and 1200°C than a corrosion layer formed under irradiation. Reduction of the pre-oxide layer is even observed at 1000°C for short oxidation durations for the O_2+steam pre-oxidized

cladding. This reduction of the pre-oxide, in terms of thickness, is linked to the examination of the radial cross-section presented in FIG 14 (b), showing a stratified structure in the metal part after steam oxidation at 1000°C.
As mentioned above, the hydrogen pickup for O_2+steam pre-oxidized specimens during the high temperature oxidation remains low, as for irradiated cladding [29].

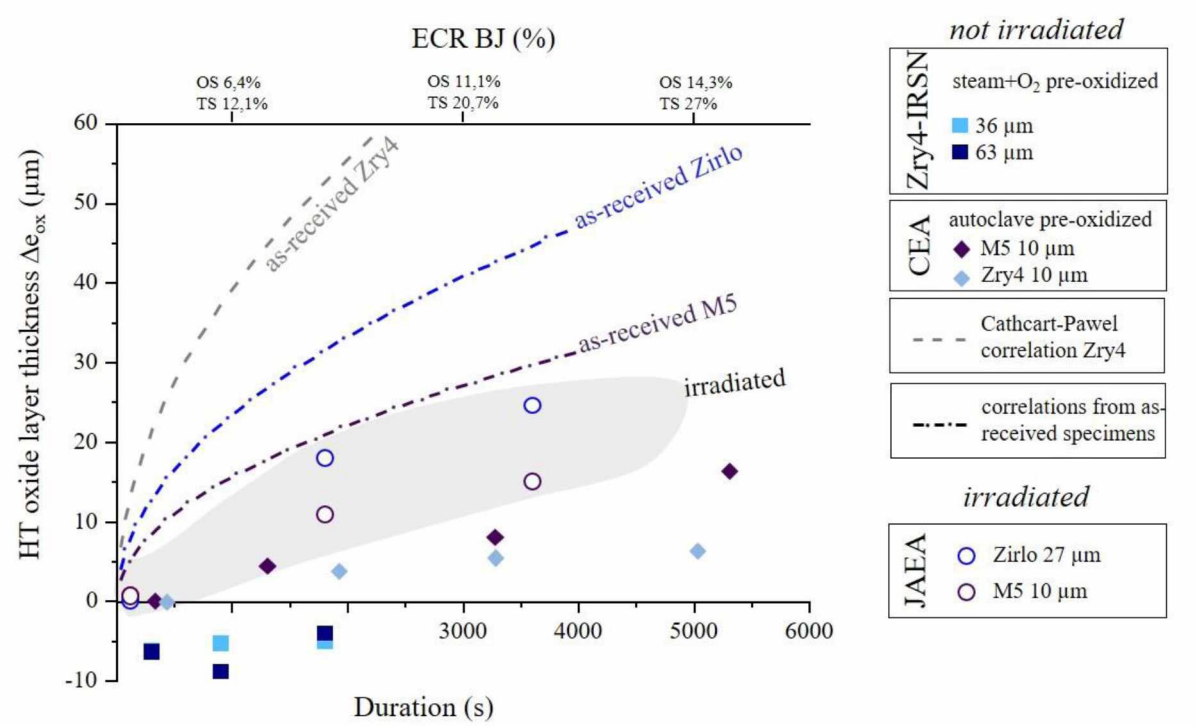

FIG 17: Thickness of the oxide layer formed during the steam oxidation at 1000°C as a function of the test duration. OS and TS stand respectively for one-side oxidation and two-side oxidation. Average trends on as-received Zirlo and M5 are established from literature data (Le Saux [5, 8], Narukawa [29]).

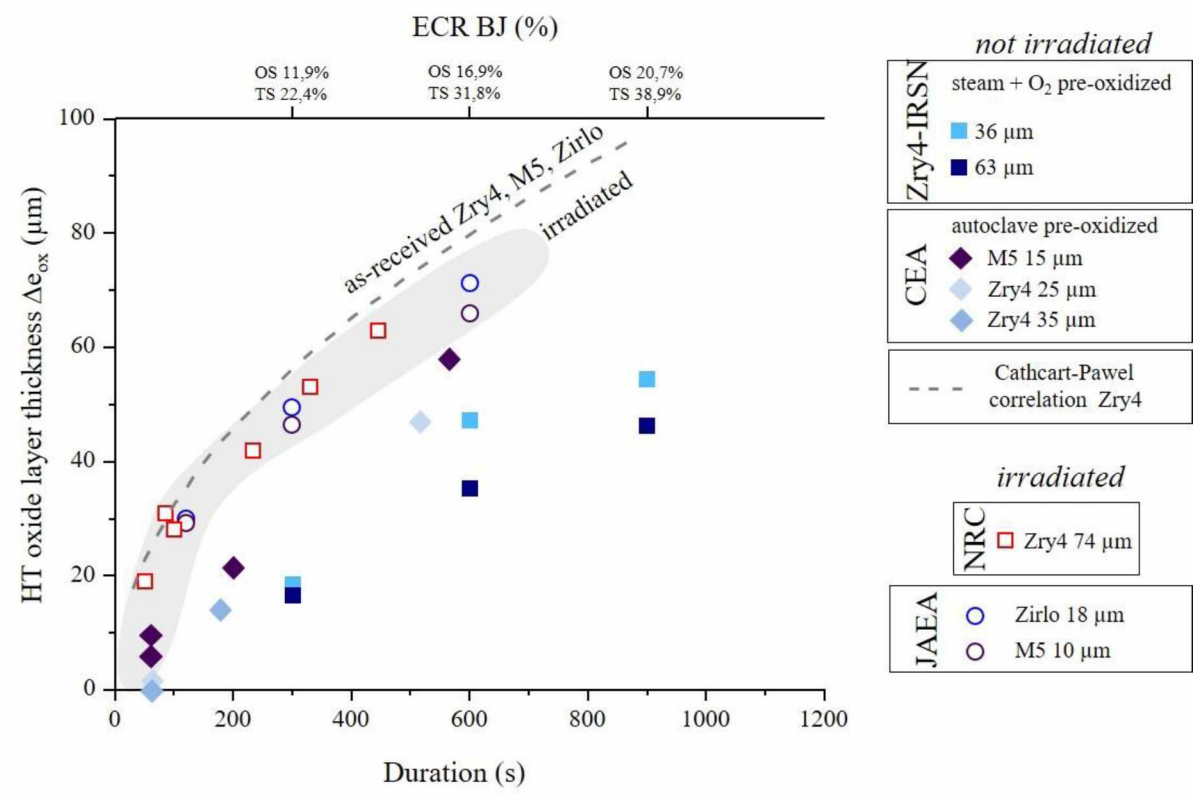

FIG 18: Thickness of the oxide layer formed during the steam oxidation at 1200°C as a function of the test duration. OS and TS stand respectively for one-side oxidation and two-side oxidation. Average trends for as-received Zirlo and M5 are established from literature data by (Le Saux [5, 8], Narukawa [29], Billone [25]).

The conditions of pre-oxidation and the microstructure of the pre-oxide undoubtedly determine the high temperature steam oxidation behavior of zirconium alloys.

Formed in laboratory or under irradiation, the oxide layer or corrosion layer shows a stratified microstructure, defined by the circumferential cracks that formed cyclically at each kinetic transition. A ~2 µm crack spacing in the radial direction is reported for Zry-4 and M5® irradiated cladding [18, 33], which is slightly lower than the strata thickness observed on Zry-4 O_2+steam pre-oxidized samples. The circumferential cracks close to the metal/oxide interface seem more opened for O_2+steam pre-oxidized samples, whereas longer and wider cracks are observed close to the water-side for irradiated cladding. Apart from the strata uniformity, micro-cracks and nano-porosities are observed under the circumferential cracks for autoclave and O_2+steam pre-oxidized samples. Many authors have studied the microstructure of the corrosion layer formed on zirconium alloys and its evolution during the growth phase, see for example ref. [20, 34-36]. As a summary of the main findings obtained so far in this domain, we have chosen to extract the following FIG 19 from ref. [36], where the formation of the successive oxide layers is shown schematically:

- in the early stages of corrosion, the oxide is characterized by small, equiaxed grains with a large range of orientations. The small grain size and the presence of high compressive stress stabilize the tetragonal phase of zirconia.
- As the oxide thickens, the corrosion rate progressively slows down, allowing time for the growth of suitably oriented tetragonal grains. Once they reach a certain size, the favorably-oriented tetragonal grains transform into monoclinic grains. Locally, differences in the crystallographic parameters and the volumic expansion due to the tetragonal/monoclinic transformation induce stresses, in addition to the stresses due to the Pilling-Bedworth ratio.
- Above a critical compressive stress level in the oxide, the metal/oxide interface partly delaminates and interface cracks form inducing a strong degradation of the oxide layer, leading to the kinetic transition with new surfaces of bare metal in the delaminated regions, and the formation of new small tetragonal grains.

These mechanisms, based on experimental examinations of autoclave-pre-oxidized cladding can probably also be extended to the oxide formed in O_2+steam at 425°C, considering the similarities between both oxide in terms of stratified microstructure, porosities, shape and size of oxide grains.
However, regarding the irradiated cladding, the neutron irradiation may changes these mechanisms by introducing vacancies homogeneously across the oxide scale and weakening the charge gradients [37]. These excess vacancies enhance the mobility of oxygen and may also relax the compressive stresses in the oxide [37]. These modifications in oxygen transport and in compressive stresses may influence the nucleation and growth of grains that grow into the metal at the M/O interface. Indeed, TEM examinations of irradiated Zry-2 show that the irradiated oxides have a more heterogeneous microstructure, with irregular grain morphology and a higher fraction of equiaxed grains [20, 38]. Regarding porosity and cracks, significant intergranular porosity is observed in irradiated cladding. The porosity increases with burnup and the pores even coalesce, resulting in significant decohesion between grains throughout the oxide (FIG 20) [18, 39]. Garner [28] suggests that reactor conditions modify significantly the oxide growth and nucleation processes, with enhancement of the nucleation rate of new oxide grains at the expanse of growing of the existing ones. It could be argued that these results were obtained in BWR, so in different conditions than PWR. Literature on irradiated Zry-4 microstructure is less extensive than on Zry-2. However, formation of randomly oriented nanocrystalline tetragonal oxide grains, leading to a highly porous oxide structure, or increase in intergranular porosity and grain decohesion away from the metal-oxide interface was also reported for Zry-4 [33, 40]. More recently, experiments on Zry4 cladding using proton irradiation show a transition from columnar to equiaxed grain shape, as the irradiation dose rate increases [37, 41].
These differences in oxide microstructure resulting from neutron irradiation in normal conditions may lead to a faster transport of oxygen at high temperature and thus may explain the less protective character of the corrosion layer formed under irradiation, when heated at high temperature in steam. Irradiation also affects the bare metal microstructure with phenomena such as dislocation loops formation, radiation-enhanced precipitation or dissolution, redistribution and reprecipitation of intermetallic phases containing Zr and elements such as Fe, Cr and Ni [42-44].

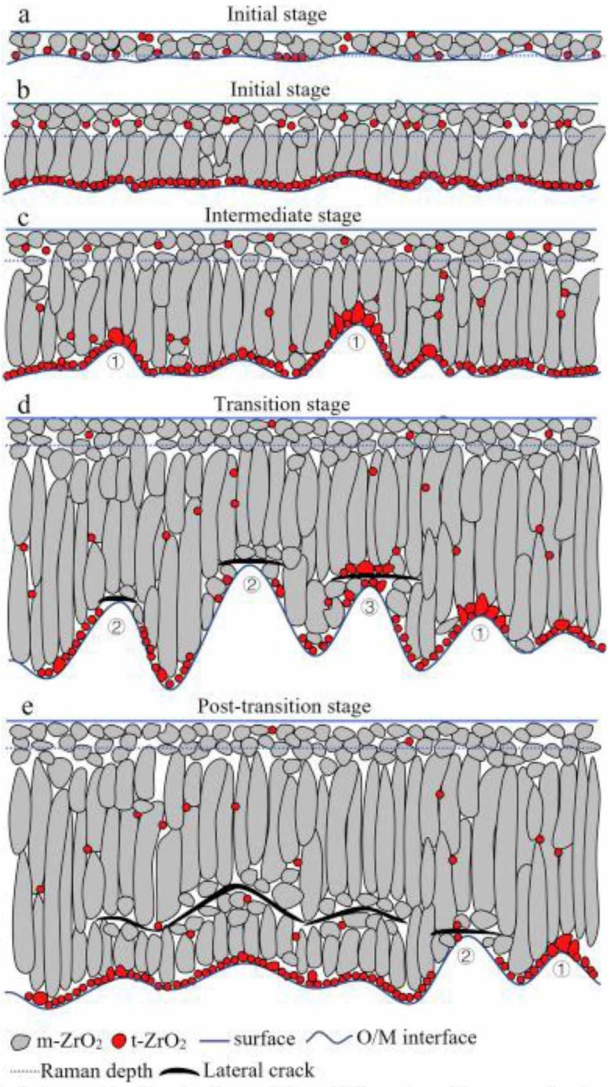

FIG 19: Schematic illustration of the different oxide growth stages [36]

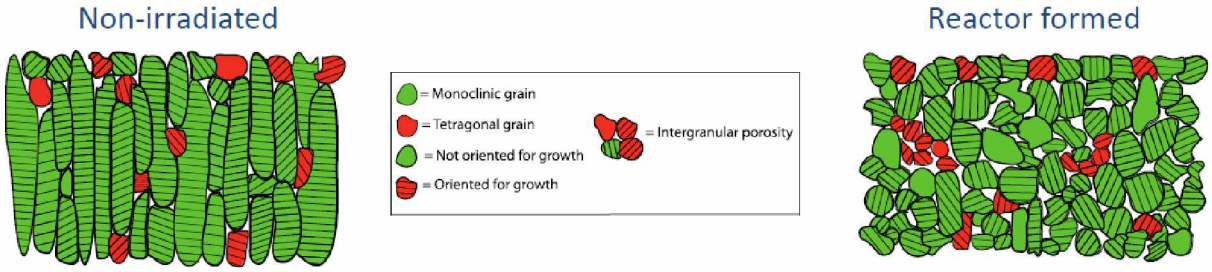

FIG 20: Schematic illustration of the microstructure of the oxide formed in autoclave or in-reactor (Reprinted with permission from A. Garner) [39]

Furthermore, in LOCA situations, one has to keep in mind the consequences of the ballooning process: due to the high metal strain level, the corrosion oxide layer cracks and between the remaining adherent oxide fragments, the bare metal is exposed to steam at regular intervals, and oxidizes like as-received material. Oxygen can diffuse crosswise, enhancing the formation of HT oxide under the pre-oxide fragments. This phenomena is illustrated in FIG 21, for irradiated Zirlo. The resulting weight gain in the balloon is thus expected to reach an intermediate value between the weight gain of as-received and pre-oxidized cladding.

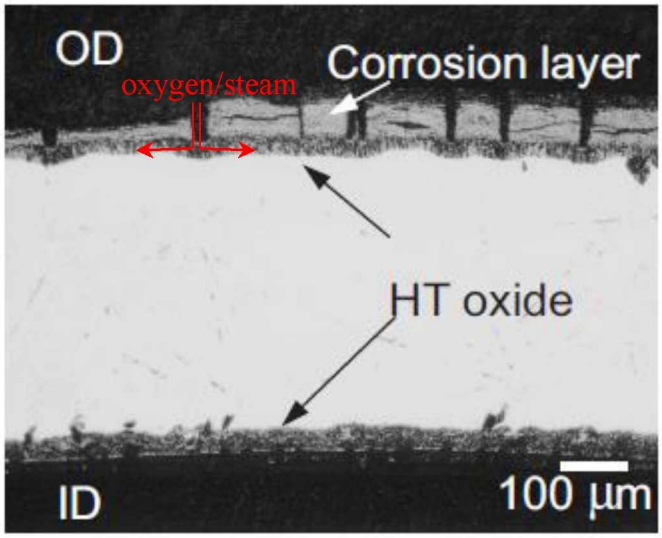

FIG 21: Radial cross-section of irradiated Zirlo after steam oxidation at 1186°C for 153s (Courtesy of JAEA) [45]

Thus, HT oxide thicknesses or weight gain obtained on as-received cladding can be considered as upper bounds of expected values on irradiated cladding. However, results obtained on as-received samples would not account for the complex influence of hydrogen picked up during the normal reactor operation. As hydrogen is a β stabilizing element for zirconium, it might influence the zirconium phase diagram and the distribution of oxygen in the cladding after a LOCA transient. So, it seems important to supplement tests on as-received samples with tests on pre-hydrided or pre-oxidized cladding, which is known to have strong consequences on the phases' distribution and cladding post-quench mechanical properties [4].

5 CONCLUSIONS

An extensive study has been carried out on the protective effect of corrosion layers with regards to the high temperature oxidation in steam during a LOCA transient. Zircaloy-4 cladding samples pre-oxidized in O_2+steam at 425°C have been oxidized in flowing steam at high temperature (900 - 1200°C) for different durations. For all tested conditions, the weight gains measured for pre-oxidized samples are lower than those obtained for bare cladding, indicating that the pre-oxide has a protective influence against extended oxidation at high temperature. Metallographic examinations of the samples after the high temperature oxidation tests confirm the protective effect of the pre-oxide layer, showing lower amounts of high temperature oxide formed when a pre-oxide layer is present. The hydrogen pickup by cladding during HT oxidation remains low for the tested conditions.

The results obtained on the O_2+steam pre-oxidized samples are in good agreement with published data on autoclave-pre-oxidized samples.

Data available in the literature on irradiated cladding show also a protective effect of the corrosion layer on oxidation. However, the pre-oxidized layer formed in laboratory, either in O_2+steam or in autoclave, has a more protective effect at 1000°C and 1200°C than a corrosion layer formed under irradiation. This difference in protectiveness may be explained by a more heterogeneous and randomly oriented grain microstructure with reduced columnar grain growth and a higher intergranular porosity under irradiation.

Further investigations are planned at IRSN to confirm these results in particular on M5® cladding, for which more experimental data are available for irradiated specimens.

As a consequence, laboratory formed oxides can be used to identify and characterize some important mechanisms affecting high temperature oxidation of irradiated and corroded claddings but do not provide results that can be quantitatively transposed to irradiated claddings. Laboratory pre-oxidation rather exacerbate the protective influence of the pre-oxide. HT oxide thicknesses or weight gain obtained on as-received cladding can be considered as upper bounds of expected values on irradiated cladding. Nevertheless,

tests on irradiated materials are considered as necessary to fully understand and describe the influence of corrosion layers.

Acknowledgements

EDF is acknowledged for careful rereading and for financial support of the present work. Authors are grateful to Michel Mermoux (University Grenoble Alpes, LEPMI, UMR 5279 CNRS) for Raman analysis of the O_2+steam and autoclave pre-oxidized samples.

References

[1] T. Fuketa, "JAERI Experimental Basis on RIA and LOCA," in *OECD/CSNI/SEGFSM meeting*, OECD headquarters, Paris, France, 2005.

[2] T. Chuto, "Oxidation of High Burnup Fuel Cladding in LOCA Conditions," in *Fuel Safety Research Meeting*, Tokai, Japan, 2010.

[3] J. H. Baek and Y. H. Jeong, "Steam Oxidation of Zr-1.5Nb-0.4Sn-0.2Fe-0.1Cr and Zircaloy-4 at 900-1200°C," *Journal of Nuclear Materials,* vol. 361, pp. 30-40, 2007.

[4] J. C. Brachet *et al.*, "Hydrogen Content, Preoxidation, and Cooling Scenario Effects on Post-Quench Microstructure and Mechanical Properties of Zircaloy-4 and M5 Alloys in LOCA conditions," in *Zirconium in Nuclear Industry: 15th International Symposium, ASTM STP 1505*, Sunriver, Oregon, 2008, vol. 5, no. 5: ASTM International, pp. 91-118.

[5] M. Le Saux, J. C. Brachet, V. Vandenberghe, D. Gilbon, J. P. Mardon, and B. Sebbari, "Influence of Pre-Transient Oxide on LOCA High Temperature Steam Oxidation and Post-Quench mechanical Properties of Zircaloy-4 and M5™ cladding," in *WRFPM 2011*, Chengdu, China, 2011.

[6] S. Leistikow, G. Schanz, and H. V. Berg, "Kinetik and Morphologie der isothermen Dampf-Oxidation von Zircaloy 4 bei 700-1300°C ", Kfk 2587, Marz 1978 1978.

[7] V. Vrtilkova, "Review of Recent work at UJP PRAHA on the LOCA Embrittlement Criterion," in *6th Plenary Meeting of the OECD/CSNI/SEGFSM*, Paris, 2005.

[8] M. Le Saux *et al.*, "Effect of a pre-oxide on the high temperature steam oxidation of Zircaloy-4 and M5Framatome alloys," *Journal of Nuclear Materials,* vol. 518, pp. 386-399, 2019/05/01/ 2019.

[9] C. Desgranges, N. Bertrand, K. Abbas, D. Monceau, and D. Poquillon, "Numerical Model for Oxide Scale Growth with Explicit Treatment of Vacancy Fluxes," *Materials Science Forum,* vol. 461-464, pp. 481-488, 2004.

[10] J. V. Cathcart *et al.*, "Zirconium Metal-Water Oxidation Kinetics IV. Reaction rate Studies," ORNL/NUREG-17, 1977.

[11] B. Mazères, C. Desgranges, C. Toffolon-Masclet, and D. Monceau, "Experimental study and numerical simulation of high temperature (1100-1250°C) oxidation of prior-oxidized zirconium alloy," *Corrosion Science,* vol. 103, pp. 10-19, 2016/02/01/ 2016.

[12] S. Guilbert, P. Lacote, G. Montigny, C. Duriez, J. Desquines, and C. Grandjean, "Effect of pre-oxide on Zircaloy-4 high temperature steam oxidation and post-quench mechanical properties," *J. ASTM Int.*, vol. STP 1543, pp. 1-27, 2014.

[13] J. C. Brachet and V. Vandenberghe, "Comments to Papers of J.H. Kim et al. [1] and M. Große et al. [2] Recently Published in JNM "On the hydrogen uptake of Zircaloy-4 and M5™ Alloys Subjected to Steam Oxidation in the 1100-1250°C Temperature Range"," *J. Nucl. Mater.*, vol. 395, no. 1-3, pp. 169-172, 2009.

[14] H. Uetsuka, "Embrittlement of Zircaloy-4 due to Oxidation in Environment of Stagnant Steam," *Journal of Nuclear Science and Technology,* vol. 19, no. 2, pp. 158-165, 1982.

[15] H. Uetsuka, "High temperature Oxidation of Zircaloy-4 in Diluted Steam," *Journal of Nuclear Science and Technology,* vol. 26, no. 2, pp. 240-248, 1989.

[16] A. J. G. Maroto *et al.*, "Growth and Characterization of Oxide Layers on Zirconium Alloys," *Journal of Nuclear Materials,* vol. 229, pp. 79-92, 1996.

[17] A. Yilmazbayhan, E. Breval, A. T. Motta, and R. J. Comstock, "Transmission Electron Microscopy Examination of Oxide Layers Formed on Zr Alloys," *Journal of Nuclear Materials,* vol. 349, no. 3, pp. 265-281, 2006.

[18] P. Bossis, D. Pêcheur, K. Hanifi, J. Thomazet, and M. Blat, "Comparison of the high Burn-Up Corrosion on M5 and low tin Zircaloy-4," in *Zirconium in the Nuclear Industry: 14th International Symposium, ASTM STP 1467*, Stockholm, Sweden, 2004: ASTM International, West Conshohocken, PA, pp. 494-524.

[19] A. Kasperski, C. Duriez, and M. Mermoux, "Combined Raman imaging and ^{18}O tracer analysis for the study of high temperature oxidation of pre-oxidized Zirclaoy-4 in spent fuel pool accident," in *18th International Symposium on Zirconium in the Nucelar Industry*, Hilton Head Island, SC, USA, 2016, vol. STP1597.

[20] A. Garner, A. Gholinia, P. Frankel, M. Gass, I. MacLaren, and M. Preuss, "The microstructure and microtexture of zirconium oxide films studied by transmission electron backscatter diffraction and automated crystal orientation mapping with transmission electron microscopy," *Acta Materialia,* vol. 80, pp. 159-171, 2014/11/01/ 2014.

[21] X. Iltis, F. Lefebvre, and C. Lemaignan, "Microstructural study of oxide layers formed on Zircaloy-4 in autoclave and in reactor Part I: Impact of irradiation on the microstructure of the zirconia layer," *Journal of Nuclear Materials,* vol. 224, no. 2, pp. 109-120, 1995/08/01/ 1995.

[22] S. Kawasaki, T. Furuta, and M. Suzuki, "Oxidation of Zircaloy-4 under High Temperature Steam Atmosphere and its effect on Ductility of Cladding," *Journal of nuclear science and technology,* vol. 15, no. 8, pp. 589-596, 1978.

[23] M. Le Saux, J.-C. Brachet, V. Vandenberghe, A. Ambard, and R. Chosson, "Breakaway oxidation of zirconium alloys exposed to steam around 1000 °C," *Corrosion Science,* vol. 176, p. 108936, 2020.

[24] Z. Hózer, C. Gyori, L. Matus, and M. Horváth, "Ductile-to-Brittle Transition of Oxidised Zircaloy-4 and E110 Claddings," *Journal of Nuclear Materials,* vol. 373, no. 1-3, pp. 415-423, 2008.

[25] M. Billone, Y. Yan, T. Burtseva, and R. Daum, "Cladding Embrittlement During Postulated Loss-of-Coolant Accidents," US-NRC, NUREG-CR-6967, 2008.

[26] M. Ozawa, T. Takahashi, T. Homma, and K. Goto, "Behavior of Irradiated Zircaloy-4 Fuel Cladding under Simulated LOCA Conditions," in *Zirconium in the Nuclear Industry: 12th International Symposium, ASTM STP 1354*, Toronto, Canada, 2000: ASTM International, West Conshohocken, PA, pp. 279-299.

[27] J. C. Brachet, J. Pelchat, D. Hamon, and R. Maury, "Mechanical Behaviour at Room Temperature and Metallurgical Study of low-tin Zy-4 and M5™ (Zr-NbO) Alloys after Oxidation at 1100°C and Quenching," in *Proceedings of the Technical Committee meeting*, Halden, Norway, 2001, pp. 139-158.

[28] S. Leistikow and G. Schanz, "Oxidation Kinetics and Related Phenomena of Zircaloy-4 Fuel Cladding Exposed to High Temperature Steam and Hydrogen-Steam Mixtures under PWR Accident Conditions," *Nuclear Engineering and Design,* vol. 103, pp. 65-84, 1987.

[29] T. Narukawa and M. Amaya, "Oxidation behavior of high-burnup advanced fuel cladding tubes in high-temperature steam," *Journal of nuclear science and technology,* vol. 56, no. 7, pp. 650-660, 2019.

[30] F. Nagase, T. Otomo, M. Tanimoto, and H. Uetsuka, "Experiments on high Burnup fuel Behavior Under LOCA Conditions at JAERI," in *Light Water Reactor Fuel Performance*, Park City, Utah, 2000: American Nuclear Society.

[31] T. Narukawa and M. Amaya, "Behavior of High-Burnup Advanced LWR Fuel Cladding Tubes," presented at the Top Fuel 2019, Seattle, USA, September 22-26, 2019, 2019.

[32] T. Chuto, F. Nagase, and T. Fuketa, "High Temperature Oxidation of Nb-Containing Zr Alloy Cladding in LOCA Conditions," *Nuclear Engineering and Technology,* vol. 41, no. 2, pp. 163-170, 2008.

[33] P. Bossis, J. Thomazet, and F. Lefevre, "Study of the Mechanisms Controlling the Oxide Growth Under Irradiation : Characterization of Irradiated Zircaloy-4 and Zr-1Nb-O Oxide Scales," in *Zirconium in the Nuclear Industry: 13rd International Symposium, ASTM STP 1423*

Annecy, France, 2001, pp. 190-221.

[34] J. Godlewski, J. P. Gros, M. Lambertin, J. F. Wadier, and H. Weidinger, "Raman Spectroscopy Study of the Tetragonal to Monoclinic Transition in Zirconium Oxide Scales and Determination of Overall Oxygen Diffusion by Nuclear Microanalysis of O^{18}," in *Zirconium in the Nuclear*

Industry: 9th International Symposium, ASTM STP 1132, Kobe, Japan, 1991: ASTM International, pp. p. 416-436.

[35] A. T. Motta *et al.*, "Microstructure and growth mechanism of oxide layers formed on Zr alloys studied with micro-beam synchrotron radiation," in *14th International Symposium on Zirconium in the NUCLEAR INDUSTRY*, Stockholm, 2005: ASTM International, pp. 205-232.

[36] J. Liao, Z. Yang, S. Qiu, Q. Peng, Z. Li, and J. Zhang, "The correlation between tetragonal phase and the undulated metal/oxide interface in the oxide films of zirconium alloys," *Journal of Nuclear Materials,* vol. 524, pp. 101-110, 2019/10/01/ 2019.

[37] M. Reyes, P. Wang, G. Was, and J. Marian, "Determination of dose rate effects on Zircaloy oxidation using proton irradiation and oxygen transport modeling," *Journal of Nuclear Materials,* vol. 523, pp. 56-65, 2019/09/01/ 2019.

[38] S. Abolhassani *et al.*, "Towards an improved understanding of the mechanisms involved in the increased hydrogen uptake and corrosion at high burnups in zirconium based claddings," in *25th Quench Workshop*, Karlsruhe, Germany, 2019.

[39] A. Garner *et al.*, "Investigating the effect of Zirconium Oxide Microstructure on Corrosion Performance: a Comparison between Neutron, Proton, and non-irradiated Oxides," in *18th International Symposium on Zirconium in the Nuclear Industry*, Hilton Head, SC, USA, 2016.

[40] X. Iltis, F. Lefebvre, and C. Lemaignan, "Microstructure Evolutions and Iron Redistribution in Zircaloy Oxide Layers: Comparative Effects of Neutron Irradiation Flux and Irradiation Damages," presented at the Zirconium in the Nucelar Industry: Eleventh International Symposium, 1996.

[41] P. Wang, K. Kanjana, D. M. Bartels, K. Gutsol, and G. S. Was, "In-situ Irradiation Accelerated Oxidation of Zircaloy-4 under proton or Electron Irradiation in PWR Primary Water," in *17th International Conference on Environmental Degradation of Materials in Nuclear Power Systems - Water Reactors*, Ottawa, Ontario,Canada, 2015.

[42] M. Griffiths, R. W. Gilbert, and G. J. C. Carpenter, "Phase instability, decomposition and redistribution of intermetallic precipitates in Zircaloy-2 and -4 during neutron irradiation," *Journal of Nuclear Materials,* vol. 150, no. 1, pp. 53-66, 1987/09/01/ 1987.

[43] M. Griffiths, "A review of microstructure evolution in zirconium alloys during irradiation," *Journal of Nuclear Materials,* vol. 159, pp. 190-218, 1988/10/01/ 1988.

[44] M. Griffiths and H. Müllejans, "A TEM study of α-phase stability in Zr-2.5 Nb pressure tubes following neutron irradiation (A TEM study of α-phase stability)," *Micron,* vol. 26, no. 6, pp. 555-557, 1995/01/01/ 1995.

[45] F. Nagase, T. Chuto, and T. Fuketa, "Behavior of high Burn-up fuel Cladding Under LOCA Conditions," *Journal of Nuclear Science and Technology,* vol. 46, no. 7, pp. 763-769, 2009.